Dynamics of Protein Relaxation in Site-Specific Mutants of Human Myoglobin[†]

David G. Lambright, Sriram Balasubramanian, and Steven G. Boxer*

Department of Chemistry, Stanford University, Stanford, California 94305-5080

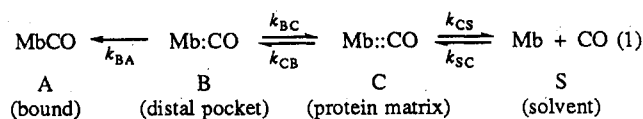Received February 22, 1993; Revised Manuscript Received June 29, 1993[●]

ABSTRACT: We have recently reported spectroscopic evidence for structural relaxation of myoglobin (Mb) following photodissociation of MbCO [Lambright, D. G., Balasubramanian, S., & Boxer, S. G. (1991) *Chem. Phys. 158*, 249–260]. In this paper we report measurements for a series of single amino acid mutants of human myoglobin on the distal side of the heme pocket (positions 45, 64, and 68) in order to examine specific structural determinants involved in this conformational relaxation and to determine the nature of the coupling between relaxation and the functional process of ligand binding. The kinetics of ligand binding and conformational relaxation were monitored by transient absorption spectroscopy in the Soret spectral region, and the results are analyzed using a four-state ligand binding model. Two principal results emerge: (1) amino acid substitutions in the distal heme pocket affect the kinetics of the nonequilibrium conformational relaxation and (2) the rate of ligand escape from the protein matrix is not significantly perturbed by the distal heme pocket mutations.

Much of our knowledge regarding the mechanism of ligand binding to myoglobin (Mb)[1] comes from extensive studies of CO rebinding to photolyzed Mb in viscous glycerol:water solutions [see for example Austin et al. (1975), Beece et al. (1980), Hasinoff (1981), Ansari et al. (1986), and Campbell et al. (1987)]. In glycerol glasses below ~200 K, the kinetics of CO rebinding to Mb are highly nonexponential, and this has been interpreted as reflecting a distribution of barrier heights for the iron–ligand bond formation step (process I; Austin et al., 1975). A variety of theoretical models have been developed to explain this basic observation (Agmon & Hopfield, 1983; Young & Bowne, 1984; Buhks & Jortner, 1985; Stein, 1985; Bialek & Goldstein, 1985; Srajer et al., 1988). In addition, several experiments indicate that the photolyzed protein is formed in a nonequilibrium distribution of conformational states (Iizuka, 1974; Ansari et al., 1985; Srajer et al., 1986; Campbell et al., 1987; Sassaroli & Rousseau, 1987; Steinbach et al., 1991). In the temperature range below the glycerol:water glass transition ($T_g \sim 180$–200 K) the time scale for relaxation to an equilibrium distribution of conformational states is long compared to the time scale for ligand rebinding (Campbell et al., 1987; Agmon, 1988; Steinbach et al., 1991; Ahmed et al., 1992). At temperatures above the glass transition relaxation occurs on the time scale of ligand rebinding (Lambright et al., 1991; Srajer & Champion, 1991; Steinbach et al., 1991; Tian et al., 1992; Ansari et al., 1992). In the temperature range between 180 and 220 K, the rebinding kinetics appear to slow down with increasing temperature (Austin et al., 1975), an observation which was originally attributed to the onset of a slower process (process II).

Agmon and Hopfield (1983) have proposed a model based on the theory of bounded diffusion perpendicular to the reaction coordinate which accounts, at least qualitatively, for these observations, including the anomalous temperature dependence. Their model also predicts a transition from multiexponential to single-exponential kinetics at temperatures above T_g where diffusive relaxation along the protein coordinate occurs on the time scale of ligand rebinding. The Agmon & Hopfield (AH) model uses a two-dimensional potential surface consisting of the iron–CO reaction coordinate, along which the motion is treated as Hamiltonian, and a generalized harmonic protein coordinate, along which the motion is treated as diffusive. Srajer, Reinisch, and Champion (1988; SRC model) have extended the concepts of the AH model by treating the iron-proximal histidine out-of-plane displacement as an independent coordinate, which is then coupled to a generalized protein coordinate that includes the remaining degrees of freedom.

Two additional processes are observed above 220 K. One of these is a bimolecular process of CO rebinding from bulk solvent (process IV; Austin et al., 1975), which is easily distinguished by its dependence on [CO]. The other is a geminate process (process III) which is characterized by single-exponential kinetics and a strong dependence on solvent viscosity (Beece et al., 1980). While processes I and II can be accounted for in the AH and SRC models, the identity of process III remains an unresolved problem. One possibility is that it corresponds to the rebinding of ligands which have migrated out of the distal heme pocket and into the protein matrix (Austin et al., 1975). With this possibility in mind, it was suggested that CO binding to myoglobin could be described by a four-state sequential reaction scheme (Dlott et al., 1983; Ansari et al., 1986):

$$\text{MbCO} \underset{k_{BA}}{\xleftarrow{\hspace{1cm}}} \text{Mb:CO} \underset{k_{CB}}{\overset{k_{BC}}{\rightleftharpoons}} \text{Mb::CO} \underset{k_{SC}}{\overset{k_{CS}}{\rightleftharpoons}} \text{Mb + CO} \quad (1)$$

$$\begin{array}{cccc} \text{A} & \text{B} & \text{C} & \text{S} \\ \text{(bound)} & \text{(distal pocket)} & \text{(protein matrix)} & \text{(solvent)} \end{array}$$

In this modification of the original reaction scheme, $k_{BA}(t)$ is a time-dependent rate for the iron–ligand bond formation step which incorporates the essential ideas of the AH model (Steinbach et al., 1991), and process III corresponds to rebinding from state C (Dlott et al., 1983; Ansari et al., 1986). In the high-temperature limit, relaxation occurs on a time scale which is short compared to ligand rebinding, and k_{BA} becomes a time-independent rate constant.
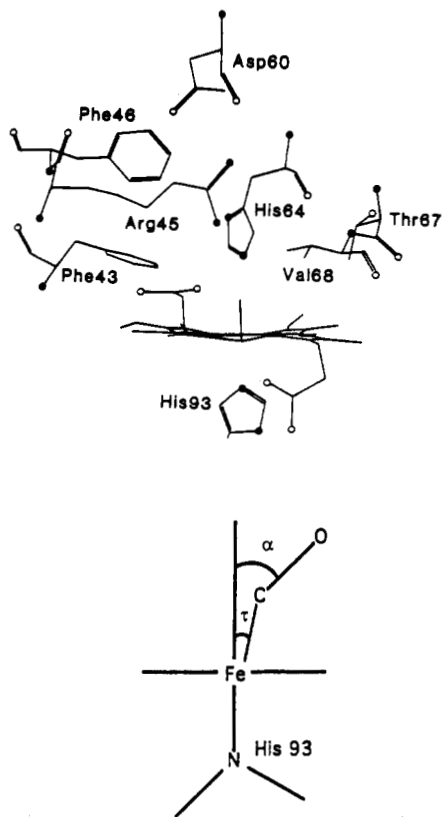
FIGURE 1: Selected residues in the region surrounding the heme in the met form of SW Mb (Tanako, 1977). The stereochemistry of these residues is essentially identical in the human Mb mutant K45R (Hubbard et al., 1990). A water molecule is weakly coordinated to the iron in this form. A expanded diagram of the geometry of the bound CO molecule in the MbCO form is shown below.

We have recently demonstrated that CO rebinding to Mb in glycerol:water solution in the temperature range from 250 to 290 K is accompanied by a small but readily detectable change in the Soret region of the photoproduct deoxyMb absorption spectrum (Lambright et al., 1991). An important observation is that the spectrum becomes identical to the equilibrium deoxyMb minus MbCO difference spectrum on a time scale which is shorter than that for process III. This spectral evolution reflects a change in the environment of the heme group due to structural relaxation of the protein. Subsequently, Ansari et al. (1992) have also observed this spectral evolution and have studied its dependence on solvent viscosity. It has also recently been suggested that these changes may be specifically associated with a relaxation in the distal heme pocket (Tian et al., 1992). Consequently, it would be interesting to know whether these changes are affected by amino acid substitutions in the distal heme pocket. In the following we present the kinetics of ligand binding and structural relaxation in several site-specific mutants of human Mb in 75% (v/v) glycerol:water solution at pH 7.0. The relevant residues are illustrated schematically in Figure 1.

EXPERIMENTAL PROCEDURES

The procedures used for preparation, expression, and purification of human Mb mutants have been described in detail (Varadarajan et al., 1989a). Wild-type human Mb contains a single Cys at position 110, in contrast with most other Mbs, which have Ala at this position. Because the presence of this Cys causes problems during purification, it has been replaced with Ala by site-specific mutagenesis. The C110A substitution does not affect the electronic absorption spectra, the NMR spectrum of the CO form, or the redox and cyanide-binding properties of the protein (Varadarajan et al., 1989a,b). There is a small change in the isoelectric point from 7.20 to 7.27 (Varadarajan et al., 1989a), and the stability of the apoprotein to denaturation by guanidinium-HCl increases by about 0.5 kcal/mol (Hughson & Baldwin, 1989). All of the mutants described in this work were prepared from a cDNA template containing the C110A substitution and, as a consequence, are double mutants. Hence, C110A replaces wild-type human Mb as the reference protein for these experiments and is referred to as WT in this paper.

The basic experimental apparatus has been described in detail (Lambright et al., 1991; Lambright, 1992). Samples of the CO derivatives of mutants in either 1-mm- or 1-cm-path-length quartz cells were photolyzed at 532 nm with 8-ns (fwhm) Q-switched pulses from the frequency-doubled output of a Nd:YAG laser (Quantel) operating at a repetition rate of 10 Hz. The energy density of the photolyzing pulses was typically 20 mJ/pulse at the sample, which produces ∼50% photolysis. A telescopic beam expander and aperture were used to improve the spatial homogeneity of the photolyzing light. Transmission changes were monitored with a CW probe beam (4.5 nm fwhm bandwidth) obtained by passing broadband light from a 500-W xenon-arc lamp through a 0.22-m monochromator. In order to eliminate the effects of photoselection, transient absorption measurements were made with the probe light polarized at the magic angle with respect to the linearly polarized excitation light. The power density of the probe beam at the sample was ∼20 μW/cm². The probe beam was detected with a 200-MHz photodiode detector constructed in this laboratory (Lambright, 1992). Scattered laser light was rejected by placing two 80-nm fwhm interference filters having a center wavelength of 400 nm (Melles Griot) in front of the detector. Transient signals were simultaneously digitized on the nanosecond and millisecond time scales using a dual time base Tektronix DSA602 digitizing oscilloscope equipped with a 600-MHz bandwidth plugin. A small reflection from the laser, detected with a <1-ns-rise-time photodiode directly terminated into 50 Ω, was used as a trigger. The instrument response, including the effect of timing jitter, had a roughly Gaussian temporal profile with a fwhm of ∼10 ns.

Transient spectra were reconstructed from single-wavelength kinetics measured at 1-nm intervals in a random order. The data collection was fully automated by using an IBM PC and software written in this laboratory to control both the oscilloscope and the monochromator. Transmitted intensities, $I(\lambda,t)$, were converted to ΔA according to

$$\Delta A(\lambda,t) = -\log_{10}[I(\lambda,t)/I_{bas}(\lambda)] \qquad (2)$$

where I_{bas} is the transmitted baseline intensity prior to the excitation pulse. Zero time was chosen to correspond to the midpoint of the trace with the highest signal to noise. In order to obtain computationally manageable data sets, the number of points in the time domain was reduced from 5100 to 256 by selecting points on a logarithmic time scale.

Maximum Entropy Rate Distributions. The data for CO rebinding to Mb exhibit a multiexponential decay law, $N(t)$, which reflects some underlying, but unknown, distribution of rates $p(k)$. The rate and time domains are related by a Laplace transform:

$$N(t) = \int_0^{k_{max}} p(k) \exp(-kt) dk \qquad (3)$$

The distribution function $p(k)$ may be continuous, discrete, or both. Given $p(k)$, it is generally straightforward to calculate $N(t)$ numerically. In the present case, however, we begin with a discretely sampled $N(t)$, which is corrupted with

measurement noise, and we seek to recover an unknown $p(k)$. It is well known that the numerical inversion of eq 3 is an ill-posed mathematical problem, particularly in the presence of noise. Consequently, there will be many feasible solutions which both satisfy the data and are physically reasonable.

It is possible, however, to select a solution from the feasible set which has no correlations in $p(k)$ except those that are required by the data. This is done by maximizing the Lagrangian function $Q = S - \lambda\chi^2$, where $\chi^2 = \Sigma_i(d_i - m_i)^2/\sigma_i^2$ is the usual misfit statistic and S is the Shannon–Jaynes entropy (Jaynes, 1983):

$$S = \Sigma_k p_k \log(p_k/m_k) \tag{4}$$

where m_k is a prior model for the distribution and

$$p_k = \frac{\int_k^{k+\Delta k} p(k)dk}{\int_0^{k_{max}} p(k)dk} \tag{5}$$

In principle, the value of the Lagrange multiplier λ is chosen such that $\chi^2 \simeq N$, where N is the number of data pairs. This solution is defined as the maximum entropy (MEM) solution.

In the present application, the MEM solution for $p(k)$ was found by using the general algorithm developed by Skilling and Bryan (1984). The transform variable k was represented by 256 points which were equally spaced on a log scale. An "ignorant" prior distribution was established by setting m_k equal to a constant, which corresponds to $m_k = k$ on a linear scale (Jaynes, 1986; Lively et al., 1986). The progress of the algorithm was monitored by calculating

$$TEST = \frac{1}{2}\left|\frac{\nabla S}{|\nabla S|} - \frac{\nabla\chi^2}{|\nabla\chi^2|}\right|^2 \tag{6}$$

Convergence was determined by two criteria, $\chi^2/N = 1.3$ and TEST < 0.01. This choice for the final χ^2/N allows for some uncertainty in the estimate of σ_i and avoids the potential problem of overfitting the data.

RESULTS AND ANALYSIS

Transient absorption kinetics on the nanosecond to millisecond time scale were acquired at many wavelengths in the Soret spectral region following photolysis of the MbCO forms of WT and site-specific mutants at His 64 (Ala, Leu, Gln, Val), Val 68 (Ala, Asn), and Lys 45 (Arg) in 75% (v/v) glycerol:water at 250, 270, 290, and 310 K. Each data set consists of a matrix, $\Delta A(\lambda,t)$, which can be viewed either as rows of transient absorption kinetics measured at different wavelengths or, equivalently, as columns of transient spectra at different times. Following the approach outlined in detail in Lambright et al. (1991), each $\Delta A(\lambda,t)$ is decomposed by singular value decomposition (SVD) into a product of three matrices:

$$\Delta A(\lambda,t) = USV^T \tag{7}$$

As shown in detail for WT (Lambright et al., 1991), for all the mutants the first two basis spectra (columns of U) and their associated time courses (columns of V) contain essentially all of the signal as determined by several criteria, including the magnitude of the singular values (diagonal elements of S) and the autocorrelation of the columns of U and V. The remaining columns of U and V represent primarily measurement noise.

The first two basis spectra and their corresponding time courses for several mutants at 250 K are shown in Figures 2–5. These basis spectra are an orthogonal representation of the spectral changes which occur subsequent to photolysis. The major spectral change, represented by U_1, can be identified
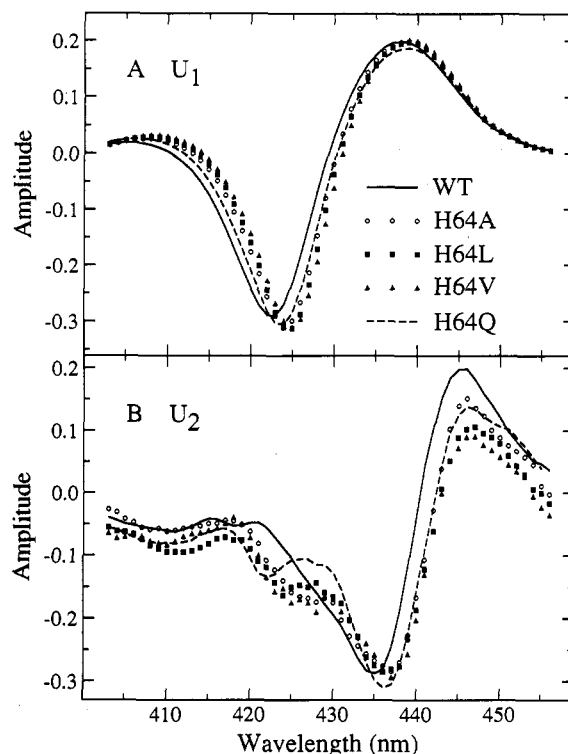

FIGURE 2: Basis spectra (columns of U) from the SVD of $\Delta A(\lambda,t)$ at 250 K for WT, H64A, H64L, H64Q, and H64V. (A) Basis spectrum (U_1) with the largest singular value. (B) Basis spectrum (U_2) with the second-largest singular value.
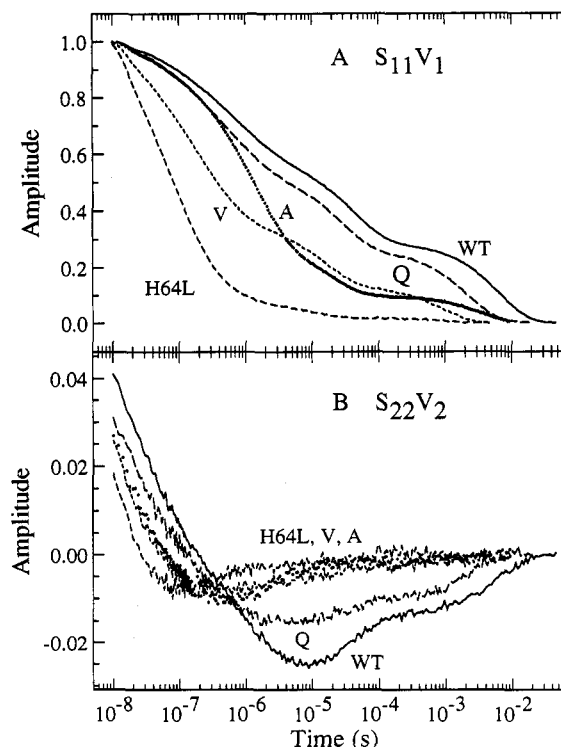

FIGURE 3: Time dependence (columns of S·V) of the basis spectra from the SVD of $\Delta A(\lambda,t)$ at 250 K for WT, H64A, H64L, H64Q, and H64V. The curves are labeled with the one-letter codes of the residues at position 64. (A) $S_{11}V_1$. (B) $S_{22}V_2$.

with the process of ligand rebinding based on the similarity of U_1 to the equilibrium deoxyMb – MbCO difference spectrum. The spectral change represented by U_2 can be identified with a small change in the photoproduct deoxyMb spectrum. This deoxyMb spectral change has been interpreted to be the result of a conformational relaxation of the protein (Lambright et al., 1991; Ansari et al., 1992).
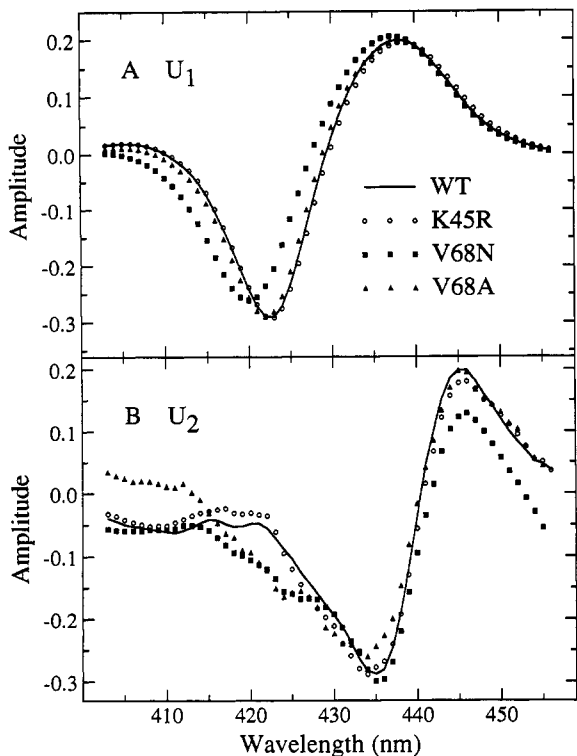
FIGURE 4: Basis spectra (columns of U) from the SVD of $\Delta A(\lambda,t)$ at 250 K for WT, K45R, V68A, and V68N. (A) Basis spectrum (U_1) with the largest singular value. (B) Basis spectrum (U_2) with the second-largest singular value.
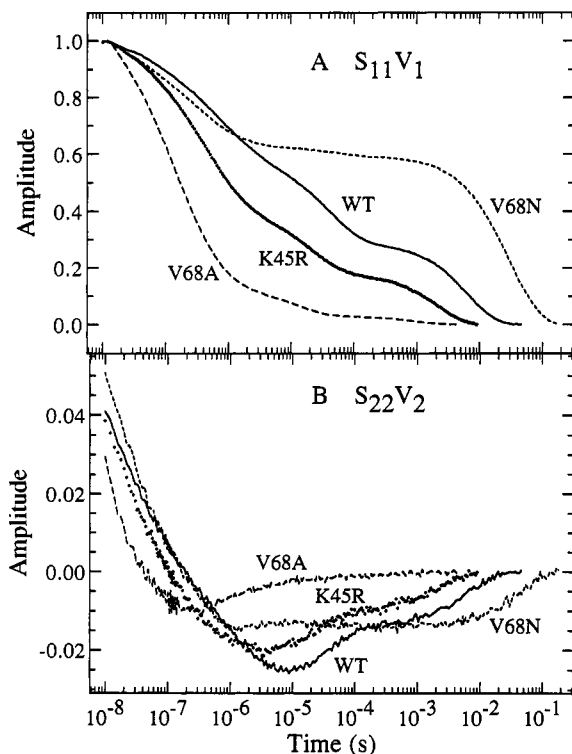

FIGURE 5: Time dependence (columns of S·V) of the basis spectra from the SVD of $\Delta A(\lambda,t)$ at 250 K for WT, K45R, V68A, and V68N. (A) $S_{11}V_1$. (B) $S_{22}V_2$.

The time dependence of the first two basis spectra was parameterized by simultaneously fitting $S_{11}V_1$ and $S_{22}V_2$ to a sum of exponentials:

$$C_i(t) = \sum_{j=1}^{n} a_{ij} \exp(k_j t) \qquad (8)$$

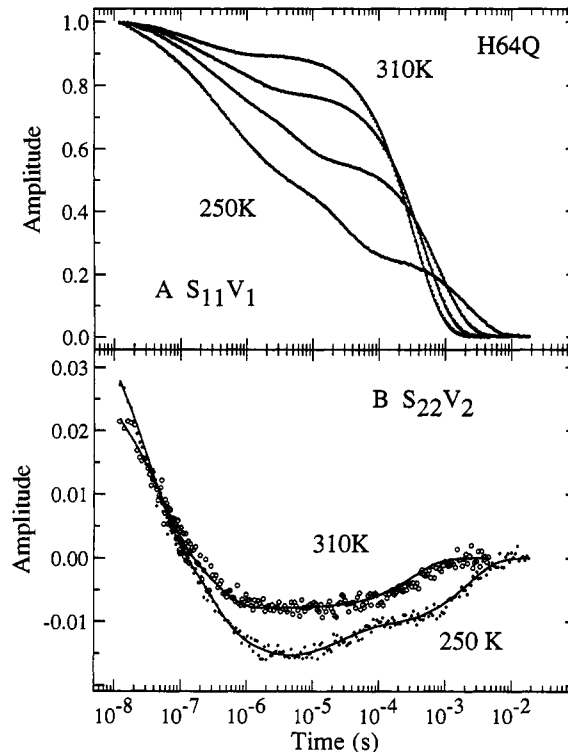where $C_i(t)$ is the model function for the ith column of S·V and n is the minimum number of exponentials required to fit

FIGURE 6: Time dependence (columns of S·V) of the basis spectra from the SVD of $\Delta A(\lambda,t)$ for H64Q. Symbols represent data, and solid lines represent the model from a simultaneous fit of $S_{11}V_1$ and $S_{22}V_2$ to a sum of exponentials. (A) $S_{11}V_1$ at 250, 270, 290, and 310 K. (B) $S_{22}V_2$ at 250 and 310 K. Intermediate temperatures were omitted for clarity.

Table I: Summary of Model Parameters for CO Rebinding to Mb Mutants in 75% (v/v) Glycerol:Water Solution with 100 mM Potassium Phosphate, pH 7.0, at 250 K

Mb	parameter	exponential component (j)				
		1	2	3	4	5
WT	a_{1j}	0.06	0.17	0.15	0.27	0.35
	a_{2j}	0.032	0.020	0.017	−0.11	−0.012
	k_j (s⁻¹)	2.2×10^7	2.7×10^6	4.2×10^5	3.2×10^4	4.5×10^2
K45R	a_{1j}	0.10	0.28	0.24	0.20	0.18
	a_{2j}	0.041	0.019	0.007	−0.011	−0.010
	k_j (s⁻¹)	3.5×10^7	4.0×10^6	8.3×10^5	4.3×10^4	4.6×10^2
H64A	a_{1j}	0.11	0.16	0.45	0.18	0.10
	a_{2j}	0.037	0.013	−0.012	−0.0023	−0.0013
	k_j (s⁻¹)	3.8×10^7	3.2×10^6	5.7×10^5	5.1×10^4	5.3×10^2
H64L	a_{1j}	0.32	0.43	0.18	0.05	0.02
	a_{2j}	0.032	0.0005	−0.0052	−0.0023	−0.0003
	k_j (s⁻¹)	5.5×10^7	9.9×10^6	2.3×10^6	1.1×10^5	9.8×10^2
H64Q	a_{1j}	0.09	0.21	0.20	0.25	0.25
	a_{2j}	0.031	0.017	0.0051	0.0050	−0.010
	k_j (s⁻¹)	3.4×10^7	3.9×10^6	6.9×10^5	3.4×10^4	4.4×10^2
H64V	a_{1j}	0.19	0.27	0.22	0.20	0.12
	a_{2j}	0.037	0.012	−0.0047	−0.0031	−0.0029
	k_j (s⁻¹)	5.7×10^7	7.4×10^6	1.7×10^6	6.3×10^4	1.1×10^3
V68A	a_{1j}	0.17	0.36	0.17	0.07	0.02
	a_{2j}	0.015	0.0064	−0.0077	−0.0024	−0.0008
	k_j (s⁻¹)	2.7×10^7	5.8×10^6	1.4×10^6	7.9×10^4	1.1×10^3

the data at each temperature. Although the value of n depends on the temperature at which the measurement is taken, it appears to be similar for the different mutants. At 250 K, $n = 5$; at 270 K and 290 K, $n = 4$; and at 310 K, $n = 3$. The results of the simultaneous fits of $S_{11}V_1$ and $S_{22}V_2$ for several of the mutants are shown in Figures 6–9. Model parameters at 250 and 290 K are presented in Tables I and II, respectively.

Because the number of kinetic intermediates exceeds the number of significant basis spectra, some of the intermediates must have essentially identical spectra (apart from changes in oscillator strength). It is useful to make the *interpretive assumption* that the magnitude of the deoxyMb spectral change
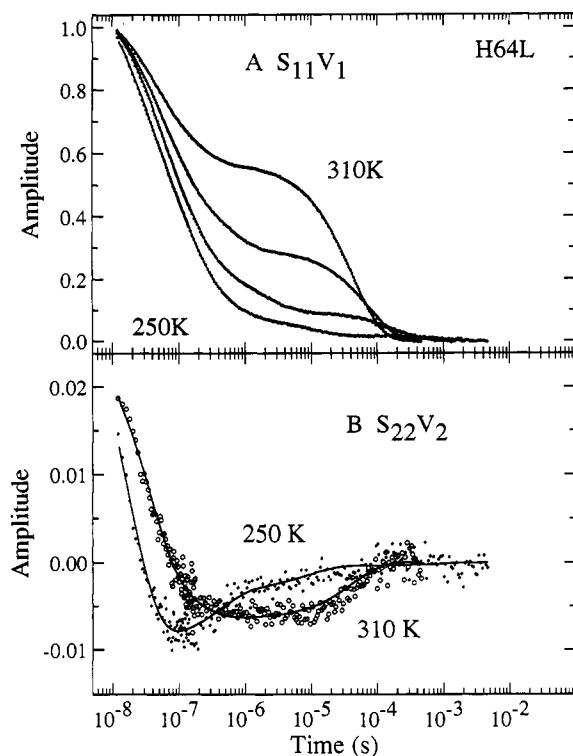
FIGURE 7: Time dependence (columns of S·V) of the basis spectra from the SVD of $\Delta A(\lambda,t)$ for H64L. Symbols represent data, and solid lines represent the model from a simultaneous fit of $S_{11}V_1$ and $S_{22}V_2$ to a sum of exponentials. (A) $S_{11}V_1$ at 250 K, 270 K, 290 K, and 310 K. (B) $S_{22}V_2$ at 250 K and 310 K. Intermediate temperatures were omitted for clarity.
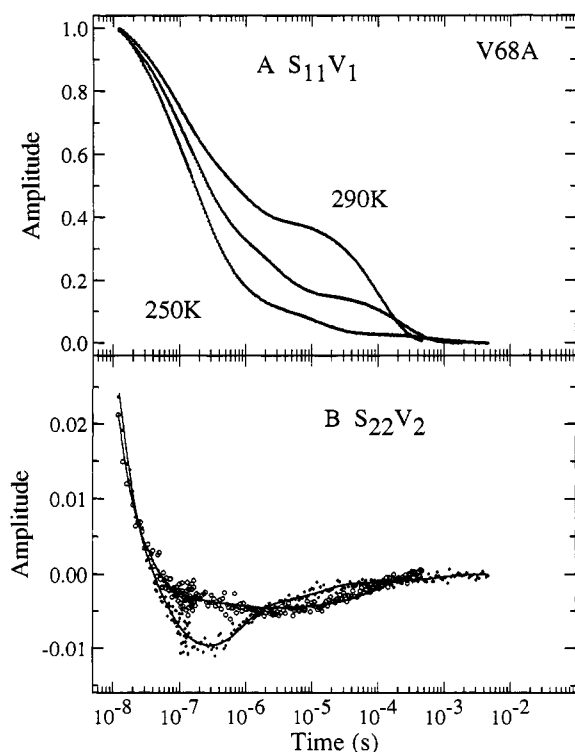

FIGURE 8: Time dependence (columns of S·V) of the basis spectra from the SVD of $\Delta A(\lambda,t)$ for V68A. Symbols represent data, and solid lines represent the model from a simultaneous fit of $S_{11}V_1$ and $S_{22}V_2$ to a sum of exponentials. (A) $S_{11}V_1$ at 250, 270, and 290 K. (B) $S_{22}V_2$ at 250 and 290 K. Intermediate temperatures were omitted for clarity.

monitors the decay of population from a set of unrelaxed conformational states having a difference spectrum $D_1(\lambda)$ into a set of relaxed conformational states having a difference
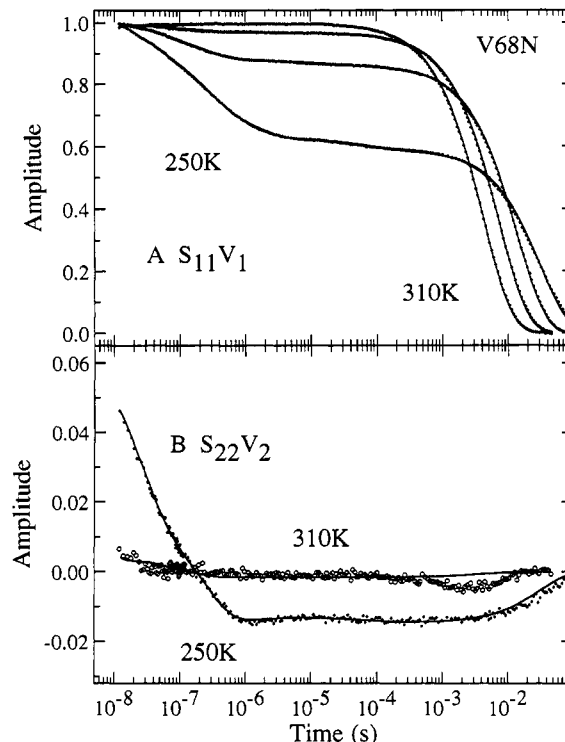

FIGURE 9: Time dependence (columns of S·V) of the basis spectra from the SVD of $\Delta A(\lambda,t)$ for V68N. Symbols represent data, and solid lines represent the model from a simultaneous fit of $S_{11}V_1$ and $S_{22}V_2$ to a sum of exponentials. (A) $S_{11}V_1$ at 250, 270, 290, and 310 K. (B) $S_{22}V_2$ at 250 and 310 K. Intermediate temperatures were omitted for clarity.

Table II: Summary of Model Parameters for CO Rebinding to Mb Mutants in 75% (v/v) Glycerol:Water Solution with 100 mM Potassium Phosphate, pH 7.0, at 290 K

Mb	parameter	exponential component (j)				
		1	2	3	4	5
WT	a_{1j}	0.01	0.05	0.09	0.85	
	a_{2j}	0.025	0.023	-0.002	-0.006	
	k_j (s^{-1})	3.2×10^7	4.8×10^6	8.3×10^5	1.4×10^3	
K45R	a_{1j}	0.05	0.09	0.12	0.74	
	a_{2j}	0.029	0.024	0.0028	-0.012	
	k_j (s^{-1})	2.9×10^7	6.1×10^6	9.2×10^5	1.8×10^3	
H64A	a_{1j}	0.011	0.21	0.14	0.64	
	a_{2j}	0.010	0.0090	0.0020	-0.0054	
	k_j (s^{-1})	4.0×10^7	5.5×10^6	1.1×10^6	3.6×10^3	
H64L	a_{1j}	0.21	0.35	0.18	0.26	
	a_{2j}	0.016	0.011	-0.0005	-0.0056	
	k_j (s^{-1})	3.8×10^7	1.1×10^7	1.8×10^6	1.3×10^4	
H64Q	a_{1j}	0.03	0.09	0.12	0.76	
	a_{2j}	0.013	0.018	0.0073	-0.011	
	k_j (s^{-1})	3.7×10^7	6.6×10^6	8.5×10^5	2.1×10^3	
H64V	a_{1j}	0.07	0.13	0.10	0.70	
	a_{2j}	0.0061	0.015	0.0045	-0.0063	
	k_j (s^{-1})	4.3×10^7	1.4×10^7	1.4×10^6	8.5×10^3	
V68A	a_{1j}	0.06	0.32	0.24	0.38	
	a_{2j}	0.023	0.0019	0.0013	-0.0043	
	k_j (s^{-1})	4.8×10^7	1.0×10^7	1.3×10^6	9.2×10^3	

spectrum $D_2(\lambda)$ which is identical to the equilibrium deoxyMb – MbCO difference spectrum. The experimental difference spectrum, $\Delta A(\lambda,t)$, is then a linear combination of $D_1(\lambda)$ and $D_2(\lambda)$:

$$\Delta A(\lambda,t) = \alpha(t)D_1(\lambda) + [N(t) - \alpha(t)]D_2(\lambda) \qquad (9)$$

where $\alpha(t)$ is the population summed over unrelaxed states, and $N(t)$ is the population of photolyzed ligands which remain unbound. From the SVD of $\Delta A(\lambda,t)$ we have

$$\Delta A(\lambda,t) = c_1(t)U_1(\lambda) + c_2(t)U_2(\lambda) \qquad (10)$$

where $c_n(t) = S_{nn}V_n(t)$. Furthermore, the $\{U_n\}$ are an

orthogonal basis for the $\{D_n\}$ which requires that

$$D_1(\lambda) = x_1 U_1(\lambda) + x_2 U_2(\lambda) \qquad (11a)$$

and

$$D_2(\lambda) = y_1 U_1(\lambda) + y_2 U_2(\lambda) \qquad (11b)$$

where x_n and y_n are constant coefficients. Combining eqs 9–11 gives

$$c_1(t) = x_1 \alpha(t) + y_1 [N(t) - \alpha(t)] \qquad (12a)$$

$$c_2(t) = x_2 \alpha(t) + y_2 [N(t) - \alpha(t)] \qquad (12b)$$

A useful property of SVD is that the $\{U_n\}$ basis has been rotated to maximize the overall contribution of U_1 to $\Delta A(\lambda, t)$ in the least-squares sense. In the limit that $D_1(\lambda) \rightarrow D_2(\lambda)$, if follows from eqs 11 and 12 that $x_1 \rightarrow y_1$, $x_2 \rightarrow y_2 \rightarrow 0$, and $c_1(t) \rightarrow y_1 N(t)$.

Assuming that all of the relaxation occurs on the time scale of our measurements, the spectrum $D_1(\lambda)$ can be calculated from

$$D_1(\lambda) \simeq C_1(t=0)U_1(\lambda) + C_2(t=0)U_2(\lambda) \qquad (13)$$

where the $C_n(t=0)$ values are determined from eq 8 using the parameters obtained from the simultaneous fits. We have shown previously for WT that the conformational relaxation is complete prior to the end of the geminate phase of rebinding (Lambright et al., 1991). This allows the spectrum $D_2(\lambda)$ to be calculated from

$$D_2(\lambda) \simeq \gamma[a_{15}U_1(\lambda) + a_{25}U_2(\lambda)] \qquad (14)$$

where $\gamma = C_1(t=0)/a_{15}$ is a correction factor for ligand rebinding, and the a_{ij} values are obtained from the simultaneous fit to eq 8. We have also used the approximation $N(t) \propto C_1(t)$. An approximation to $\alpha(t)$ is calculated by finding the linear combination of $D_1(\lambda)$ and $D_2(\lambda)$ (eq 9) which best fits the observed transient spectrum at each time. The resulting $\alpha(t)$ for different mutants at 250 K is shown in Figure 10. Because the kinetics of this relaxation are not single exponential, we parameterize the relaxation kinetics by fitting the relaxation curves in Figure 10 to a stretched exponential function:

$$\alpha(t) = \alpha_0 \exp(-k_r t)^\beta \qquad (15)$$

where the "rate constant" of relaxation k_r and the initial amplitude α_0 were allowed to vary freely, while the exponent was fixed for all of the mutants at the value ($\beta = 0.35$) obtained from the fit for WT. The parameters for the stretched exponential fit are presented in Table III. Although the parameter α_0 determines the initial amplitude of the stretched exponential model, its magnitude depends on several factors, including the concentration of the sample, the fraction photolyzed, and the extinction coefficients for the difference spectra $D_1(\lambda)$ and $D_2(\lambda)$. Therefore, the values of α_0 can not be meaningfully compared and consequently are not included in Table III. Instead the data plotted in Figure 10 have been scaled to $\alpha(0) = 1$ to facilitate meaningful comparison. These results demonstrate that the kinetics of conformational relaxation are altered by site-specific mutations at His 64 and Val 68.

Because the magnitude of the deoxyMb spectral change is small compared to the spectral change due to ligand rebinding, $S_{11}V_1$ is expected to provide a good approximation to $N(t)$. This assertion is supported by the observation that the kinetics of $S_{11}V_1$ are very similar to the kinetics measured near the wavelength of the maximum bleach ($\sim$423 nm). The largest contribution to the kinetics in this region comes from the
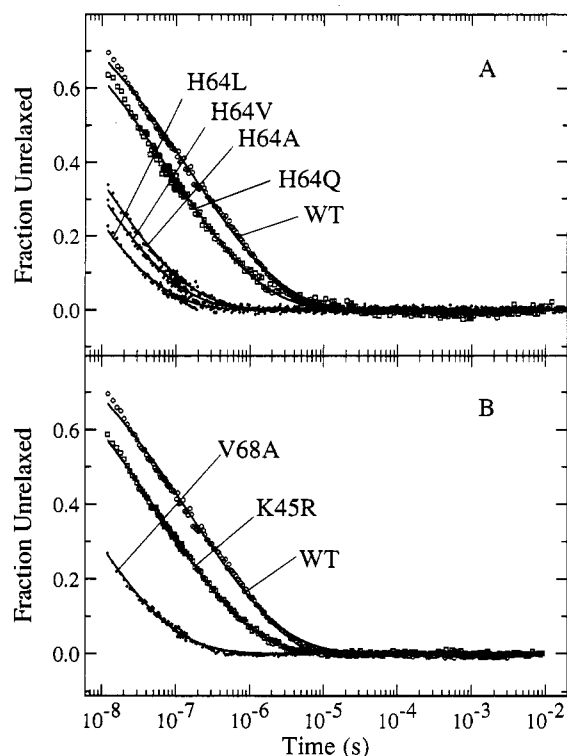

FIGURE 10: Kinetics of conformational relaxation in human Mb mutants. Time courses for the nonequilibrium conformational relaxation are shown in panel A for WT, H64A, H64L, H64V, and H64Q and in panel B for WT, V68A, and K45R. The time courses were fit to a stretched exponential model function (solid lines). The parameters k_r and α_0 were determined independently for each mutant while the exponent was fixed at the value $\beta = 0.35$ obtained from the fit for WT. Both the time courses and the model functions have been renormalized to give $\alpha_0 = 1$.

Table III: Relaxation Rates, k_r, at 250 K for the Fit of a Stretched Exponential Function (eq 15) to the Estimated Time Courses for Conformational Relaxation (Figure 10)

Mb	k_r (s^{-1})	Mb	k_r (s^{-1})
WT	6×10^6	H64Q	1×10^7
K45R	2×10^7	H64V	2×10^8
H64A	1×10^8	V68A	2×10^8
H64L	3×10^8		

recovery of the bleach of the ground-state absorption of the MbCO band due to ligand rebinding. Consistent with this, the kinetics in this region are essentially wavelength independent.

For first-order and pseudo-first-order kinetic processes, the time domain observable $N(t)$ can be related to an underlying rate distribution of rate constants, $p(k)$, by a Laplace transform (eq 3). Although direct numerical inversion of eq 3 is an ill-conditioned problem, the maximum entropy method (MEM) can be used to find a discretized distribution, $p(k_i)$, which is a feasible solution to eq 3. The MEM solution has the property that it introduces the least correlation between different members of the distribution. MEM distributions, $p(k)$, calculated from $S_{11}V_1$ for several different mutants at 250 K, are shown in Figure 11. The vertical bars in Figure 11 indicate the rates and relative amplitudes obtained from the simultaneous fits (Table I). In general, there is a correlation between the peaks in the MEM distribution and the values of the rate constants obtained from the simultaneous fits, although rate constants of similar magnitude are not resolved in the MEM distributions. In all cases, it is clear that the two slowest peaks correspond to well-resolved single-exponential processes. The slowest peak can be identified
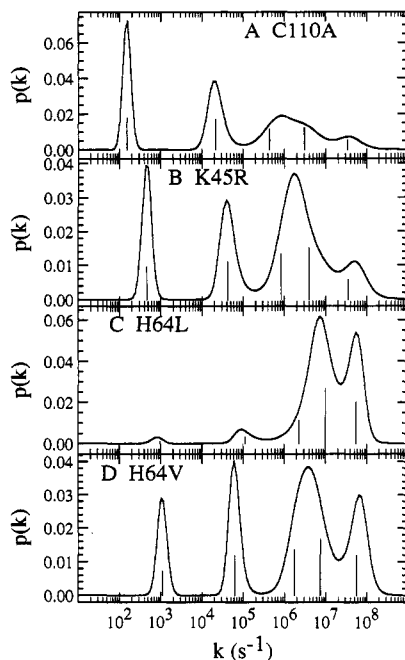
FIGURE 11: MEM rate distributions, $p(k)$, for CO rebinding at 250 K to (A) WT, (B) K45R, (C) H64L, and (D) H64V. The vertical lines represent the rate constants and relative amplitudes from the simultaneous fit of $S_{11}V_1$ and $S_{22}V_2$ to a sum of exponentials.

Table IV: Activation Parameters for CO Rebinding to Mb Mutants in 75% (v/v) Glycerol:Water Solution with 100 mM Potassium Phosphate, pH 7.0

	k_{CA}		k_{CS}		k_{SC}	
Mb	A (s^{-1})	E_a (kJ mol^{-1})	A (s^{-1})	E_a (kJ mol^{-1})	A (s^{-1})	E_a (kJ mol^{-1})
WT	4×10^9	26	1×10^{16}	56	4×10^{14}	40
K45R	8×10^9	26	8×10^{15}	56	2×10^{14}	39
H64A	3×10^9	24	2×10^{16}	57	2×10^{16}	49
H64L	3×10^{11}	31	1×10^{16}	55	8×10^{15}	45
H64Q	2×10^{10}	29	8×10^{15}	56	5×10^{14}	40
H64V	5×10^8	20	1×10^{16}	56	4×10^{17}	53
V68A	4×10^{11}	33	1×10^{16}	56	2×10^{15}	42

with bimolecular rebinding from the solvent (process IV), while the second-slowest peak can be identified with process III.

Processes III and IV (exponential components 4 and 5, respectively, in Tables I and II) correspond to ligand rebinding processes in the relaxed conformation (see Figures 7 and 10). Because these processes are relatively well resolved, the approximate relations

$$\phi_C = a_{14}/(a_{14} + a_{15}) \simeq k_{CA}/(k_{CA} + k_{CS}) \quad (16a)$$

$$k_4 \simeq k_{CA} + k_{CS} \quad (16b)$$

$$k_5 \simeq k_{SC}\phi_C[CO] \quad (16c)$$

are valid and were used to calculate the rate constants k_{CS} and k_{SC} and the apparent rebinding rate constant k_{CA} for the sequential reaction scheme (eq 1). Rate constants were determined from the data measured at 250, 270, 290, and 310 K. Activation parameters obtained from the linear least-squares fit to the Arrhenius law,

$$k = A \exp(-E_a/RT) \quad (17)$$

are presented in Table IV. An unexpected result is that the activation parameters for the rate constant of escape from the protein matrix (k_{CS}) are identical for WT and all of the distal pocket mutants.

DISCUSSION

We have modeled the data by simultaneously fitting $S_{11}V_1$ and $S_{22}V_2$ to a sum of exponentials (eq 8). Two of the exponential components ($j = 4$ and $j = 5$ in Tables I and II) correspond to well-resolved processes in the time course for ligand rebinding (see Figures 3, 5, and 11). In particular, component 5 is easily identified as the bimolecular process on the basis of its dependence on [CO] (Austin et al., 1975; Balasubramanian et al., 1993a). Under the conditions of our experiments ([CO] ≫ [Mb]), the bimolecular process is pseudo first order. Component 4 is best resolved at the lowest temperature (250 K) and corresponds to process III in sperm whale Mb (Austin et al., 1975; Beece et al., 1980). The remaining one to three exponentials (the number depending on the temperature) account for the initial nonexponential phase of the geminate rebinding. Component 1 is observed at 250 K, but not at higher temperatures, and corresponds to a partially resolved peak in the MEM rate distributions (Figure 11).

An evolution in the shape of the photoproduct deoxyMb absorption spectrum has been used to monitor the kinetics of a conformational relaxation. An unexpected but interesting result is that single amino acid substitutions on the distal side of the heme pocket alter the kinetics of this conformational relaxation (Figure 10 and Table III). In particular, k_r increases by about 1 order of magnitude for the substitutions H64A, H64V, H64L, and V68A and ~2-fold for H64Q and K45R relative to WT. It is likely that the small effect produced by the K45R substitution reflects an interaction between Arg 45 and His 64 (Balasubramanian et al., 1993c). These results require that the conformational relaxation involve residues in the distal heme pocket.

Because the experimentally determined quantity $\alpha(t)$ represents the total population in unrelaxed conformational states, it is possible that ligand binding from unrelaxed states contributes to the observed decay of $\alpha(t)$. Although this mechanism has been shown to be responsible for the spectral evolution of a near-IR charge-transfer band in Hb at cryogenic temperatures (Campbell et al., 1987; Agmon, 1988), it appears that relaxation is the dominant mechanism for spectral evolution above about 220 K for both the near-IR band (Ahmed et al., 1991) and the Soret band (Tian et al., 1992). Consistent with this interpretation is our observation that the mutants H64A, H64L, H64V, and V68A have similar time scales for spectral evolution, despite having very different ligand binding kinetics. Thus, the available evidence favors relaxation as the dominant mechanism responsible for the decay of $\alpha(t)$ in the temperature range above about 220 K.

High-resolution X-ray crystal structures for MbCO (Kuriyan et al., 1986) and deoxyMb (Takano, 1977b) reveal structural differences in the heme geometry as well as conformational differences involving residues on both the proximal and the distal side of the heme pocket. In MbCO, the heme ring has a planar geometry with the iron atom in the plane of the heme ring, whereas in deoxyMb the heme ring is domed, and the iron atom is displaced to the proximal side of the heme ring by ~0.5 Å. The proximal conformational differences consist primarily of a tilting of the proximal histidine and a displacement of the F-helix which occurs in conjunction with the iron out-of-plane displacement. In addition to global changes, the differences on the distal side include the presence of an ordered water molecule in the distal heme pocket of deoxyMb, which is excluded from the distal heme pocket in MbCO, as well as the presence of a bound ligand in MbCO that exists in several distinct conformations.

FTIR experiments on sperm whale MbCO have identified at least three CO stretch bands corresponding to different conformational states (Makinen et al., 1979; Shimada et al., 1982) which have different structures (Ormos et al., 1988) and different rebinding kinetics (Ansari et al., 1987). Following the notation of Ansari et al. (1987), these different conformational states are referred to as A substates. The distribution of the population among the three major A substates (A_0, A_1, and A_3) is a function of several variables, including temperature, solvent, and pH (Shimada et al., 1982; Ansari et al., 1987). In particular, the population in A_0 increases with decreasing temperature and decreasing pH. It has been proposed that A_0 corresponds to an open conformation of the distal heme pocket which predominates at low pH when the distal histidine is protonated, while A_1 corresponds to the closed conformation which predominates at neutral pH when the distal histidine is unprotonated (Morikis et al., 1989). The time scale for interconversion of the A substates also depends strongly on temperature and solvent viscosity. At 250 K in 75% (v/v) glycerol:water, interconversion occurs on the microsecond time scale (Young et al., 1991).

Because distal heme pocket mutations alter the kinetics for conformational relaxation, we can rule out the proposition that the structural changes involve only proximal residues. Thus, the conformational relaxation might reflect either localized structural changes in the distal heme pocket or more global changes involving both proximal and distal residues. If the changes are global, then the deoxyMb spectral evolution might be coupled to the conformational changes via the iron–proximal histidine linkage. If the changes are localized in the distal heme pocket, on the other hand, then it is less clear how the spectral evolution and the conformational changes are coupled.

A simple explanation for the effect of distal amino acid substitutions on the kinetics of conformational relaxation can be given if the relaxation depends on the photolyzed conformational substates in deoxyMb. These have been designated B substates, and they correspond to the A substates in MbCO. The A substates have an equilibrium distribution which reflects the interactions of the bound CO with distal residues, in particular Val 68 and His 64. These interactions are absent in deoxyMb, and so it is expected that the equilibrium distribution of the B substates will differ from that of the A substates. Photolysis of the iron–CO bond with a short laser pulse projects the equilibrium distribution of A substates onto a nonequilibrium distribution of B substates, which then relaxes toward equilibrium. Each of these photolyzed B substates has a unique relaxation rate. Substitutions at Val 68 and His 64 alter the interactions between these residues and the bound CO, giving rise to a different set of A substates which have different relaxation and interconversion rates.

This explanation requires that the distal substitutions alter the structures or at least the distribution of the conformational states associated with CO binding. These changes should therefore be reflected in the IR spectrum as differences in either the CO stretch frequencies or the amplitudes of the peaks corresponding to different CO stretch frequencies, or both. In fact, detailed studies of the CO forms of these mutants by FTIR spectroscopy in 75% glycerol:water solutions as a function of temperature provide support for this suggestion (Balasubramanian et al., 1993b). At 250 K, at least two CO stretch peaks are observed in the FTIR spectrum for WT: a large-amplitude peak at $\sim$1945 cm^{-1} and a small-amplitude peak at $\sim$1970 cm^{-1}. In H64L and H64V, on the other hand, a single narrow peak is observed at $\sim$1970 cm^{-1}, while in H64A two overlapping peaks centered at $\sim$1970 cm^{-1} are

observed. Thus, there is a correlation between the kinetics for conformational relaxation and the CO stretch frequencies and amplitudes in the His 64 mutants. Specifically, mutants having a single CO stretch peak centered at $\sim$1970 cm^{-1} also exhibit an increased rate of conformational relaxation relative to WT. This observation supports the hypothesis that the conformational changes involve the relaxation of a nonequilibrium distribution of photolyzed A substates.

An alternative explanation might be given in terms of the solvent reorganization which allows a water molecule to enter the heme pocket. This process should also depend strongly on solvent viscosity and could easily be affected by distal heme pocket mutations, especially if the mutations alter the solvent accessibility of the heme pocket. Replacing His 64 with smaller hydrophobic residues eliminates the hydrogen-bonding interaction which stabilizes the water molecule in the heme pocket and could increase the rate at which solvent molecules enter the heme pocket. However, it is difficult to explain why replacing Val 68 with Ala would have roughly the same effect on the kinetics of solvent reorganization as the His 64 substitutions.

CO binding to Mb can be described by a four-state reaction scheme (eq 1). It is clear that the initial phase of geminate rebinding is complex, involving both the formation of state B in a nonequilibrium distribution of conformational states and the subsequent relaxation to equilibrium. Two additional processes are observed after the initial photoproduct conformational state has relaxed to equilibrium. One of these is a geminate process (rebinding from state C) which appears to correspond to process III observed in sperm whale Mb at lower temperatures (Austin et al., 1975), while the other process corresponds to bimolecular rebinding from the solvent (state S). It has been suggested that process III corresponds to the geminate rebinding of CO molecules which have either diffused into the protein matrix or have been trapped at the protein/solvent interface (Dlott et al., 1983; Ansari et al., 1986). Alternatively, this process might simply result from the rebinding of CO in the heme pocket to the relaxed conformation of deoxyMb without the need to invoke a matrix process at all. The activation parameters in Table IV clearly demonstrate that the barrier to escape from state C does not depend on the distal pocket mutations. This result is consistent with the interpretation that process III is either a matrix or a protein/solvent interface process which does not involve the residues Val 68, His 64, or Arg 45. In contrast, the activation parameter for formation of C from S (k_{SC}) does depend on distal pocket mutations. These results are difficult to understand in terms of the sequential reaction scheme but can be rationalized if ligand diffusion between the heme pocket and the solvent involves two or more pathways, as suggested by recent molecular dynamics simulations (Elber & Karplus, 1990). We propose that process III reflects rebinding/escape of ligands which have migrated to internal cavities in the protein matrix other than the distal heme pocket.

In conclusion, it has been demonstrated that distal heme pocket mutations alter the kinetics of a conformational relaxation. We have proposed that the nonequilibrium conformational state reflects interactions between distal residues and CO which are present in MbCO but not in deoxyMb. Substitutions at His 64 and Val 68 alter these interactions and thereby influence the kinetics of conformational relaxation. This hypothesis is supported by the observation of a correlation between changes in the kinetics for conformational relaxation and changes in the distribution of A substates for different mutants (Balasubramanian et al., 1993b). Finally, the effects of distal heme pocket substitutions

on the escape kinetics are not easily interpreted in terms of a purely sequential reaction scheme but can be rationalized if ligand diffusion between the heme pocket and solvent involves multiple pathways.

REFERENCES

Agmon, N. (1988) *Biochemistry 27*, 3507–3511.

Agmon, N., Hopfield, J. J. (1983) *J. Chem. Phys. 79*, 2042–2053.

Ahmed, A. M., Campbell, B. F., Caruso, D., Chance, M. R., Chavez, M. D., Courtney, S. H., Friedman, J. M., Iben, I. E. T., Ondrias, M. R., & Yang, M. (1991) *Chem. Phys. 158*, 329–351.

Ansari, A., Berendzen, J., Bowne, S. F., Frauenfelder, H., Iben, I. E. T., Sauke, T. B., Shyamsunder, E., & Young, R. D. (1985) *Proc. Natl. Acad. Sci., U.S.A. 82*, 5000–5004.

Ansari, A., DiIorio, E. E., Dlott, D. D., Frauenfelder, H., Iben, I. E. T., Langer, P., Roder, H., Sauke, T. B., & Shyamsunder, E. (1986) *Biochemistry 25*, 3139–3146.

Ansari, A., Berendzen, J., Braunstein, D., Cowen, B. R., Frauenfelder, H., Hong, M. K., Iben, I. E. T., Johnson, J. B., Ormos, P., Sauke, T. B., Scholl, R., Schulte, A., Steinbach, P. J., Vittitow, J., & Young, R. D. (1987) *Biophys. Chem. 26*, 337–355.

Ansari, A., Jones, C. M., Henry, E. R., Hofrichter, J., Eaton, W. A., & Szabo, A. (1991) *Biophys. J. 59*, 286a.

Ansari, A., Jones, C., Henry, E. R., Hofrichter, J., & Eaton, W. A. (1992) *Science 256*, 1796–1798.

Antonini, E., & Brunori, M. (1971) *Hemoglobin and Myoglobin and their Reactions with Ligands*, North-Holland Publishing Co., Amsterdam.

Austin, R. H., Beeson, K. W., Eisenstein, L., Frauenfelder, H., & Gunsalus, I. C. (1975) *Biochemistry 14*, 5355–5373.

Balasubramanian, S., Lambright, D. G., Marden, M. C., & Boxer, S. G. (1993a) *Biochemistry 32*, 2202–2212.

Balasubramanian, S., Lambright, D. G., & Boxer, S. G. (1993b) *Proc. Natl. Acad. Sci. U.S.A. 90*, 4718–4722.

Balasubramanian, S., (1993c) Ph.D. Thesis, Stanford University, Stanford, CA.

Beece, D., Eisenstein, L., Frauenfelder, H., Good, D., Marden, M. C., Reinisch, L., Reynolds, A. H., Sorensen, L. B., & Yue, K. T. (1980) *Biochemistry 19*, 5147–5157.

Bialek, W., & Goldstein, R. F. (1985) *Biophys. J. 48*, 1027–1044.

Braunstein, D., Ansari, A., Berendzen, J., Cowen, B. R., Egeberg, K. D., Frauenfelder, H., Hong, M. K., Ormos, P., Sauke, T. B., & Scholl, R. (1988) *Proc. Natl. Acad. Sci. U.S.A. 85*, 8497–8591.

Buhks, E., & Jortner, J. (1985) *J. Chem. Phys. 83*, 4456–4462.

Campbell, B. F., Chance, M. R., & Friedman, J. M. (1987) *Science 238*, 373–376.

Carver, T. E., Olson, J. S., Smerdon, S. J., Krzywda, S., Wilkinson, A. J., Gibson, Q. H., Blackmore, R. S., Dez Ropp, J., & Sligar, S. G. (1991) *Biochemistry 30*, 4697–4705.

Case, D. A., & Karplus, M. (1979) *J. Mol. Biol. 132*, 344–368.

Case, D. A., & McCammon, J. A. (1986) *Ann. N.Y. Acad. Sci. 482*, 222.

Cheng, X., & Schoenborn, B. (1991) *J. Mol. Biol. 220*, 381–399.

Dlott, D. A., Frauenfelder, H., Langer, P., Roder, H., & DiIorio, E. E. (1983) *Proc. Natl. Acad. Sci. U.S.A. 80*, 6239–6243.

Elber, R., & Karplus, M. (1990) *J. Am. Chem. Soc. 112*, 9161–9175.

Gibson, Q. JH. (1956) *J. Physiol. 136*, 112–122.

Hasinoff, B. B. (1981) *J. Phys. Chem. 85*, 526–531.

Henry, E. R., Sommer, J. H., Hofrichter, J., & Eaton, W. A. (1983) *J. Mol. Biol. 166*, 443–451.

Hofrichter, J., Sommer, J. H., Henry, E. R., & Eaton, W. A. (1983) *Proc. Natl. Acad. Sci. U.S.A. 80*, 2235–2239.

Hofrichter, J., Henry, E. R., Sommer, J. H., Deutsch, R., Ikeda-Saito, M., Yonetani, T., & Eaton, W. A. (1985) *Biochemistry 24*, 2667–2679.

Hubbard, S. W., Hendrickson, W. A., Lambright, D. G., & Boxer, S. G. (1990) *J. Mol. Biol. 213*, 215–218.

Hughson, F. M., & Baldwin, R. L. (1989) *Biochemistry 28*, 4415–4422.

Jaynes, E. T. (1986) Maximum Entropy and Bayesian Methods, in *Applied Statistics* (Justice, J. H., Ed.) pp 26–58, Cambridge University Press, Cambridge.

Kottalam, J., & Case, D. A. (1988) *J. Am. Chem. Soc. 110*, 7690–7697.

Kuriyan, J., Wilz, S., Karplus, M., & Petsko, G. A. (1986) *J. Mol. Biol. 192*, 133–154.

Lambright, D. G., Balasubramanian, S., & Boxer, S. G. (1989) *J. Mol. Biol. 207*, 289–299.

Lambright, D. G., Balasubramanian, S., & Boxer, S. G. (1991) *Chem. Phys. 158*, 249–260.

Livesly, A. K., Licinio, P., & Delaye, M. (1986) *J. Chem. Phys. 84*, 5102–5107.

Murray, L. P., Hofrichter, J., Henry, E. R., Ikeda-Saito, M., Kitagishi, K., Yonetani, T., & Eaton, W. A. (1988) *Proc. Natl. Acad. Sci. U.S.A. 85*, 2151–2155.

Skilling, J., & Bryan, R. K.)1984) *Mon. Not. R. Astron. Soc. 211*, 111–124.

Srajer, V., & Champion, P. M. (1991) *Biochemistry 30*, 7390–7402.

Srajer, V., Schomaker, K. T., & Champion, P. M. (1986) *Phys. Rev. Lett. 57*, 1267–1270.

Srajer, V., Reinisch, L., & Champion, P. M. (1988) *J. Am. Chem. Soc. 110*, 6656–6670.

Steinbach, P. J., Ansari, A., Berendzen, J., Braunstein, D., Chu, K., Cowen, B. R., Ehrenstein, D., Frauenfelder, H., Johnson, J. B., Lamb, D. C., Luck, S., Mourant, J. R., Nienhaus, G. U., Ormos, P., Philipp, R., Xie, A., & Young, R. D. (1991) *Biochemistry 30*, 3988–4001.

Takano, T. (1977a) *J. Mol. Biol. 110*, 537–568.

Takano, T. (1977b), *J. Mol. Biol. 110*, 569–584.

Tian, W. D., Sage, J. T., Srajer, V., & Champion, P. M. (1992) *Phys. Rev. Lett. 68*, 408–411.

Tilton, R. F., Jr., Kuntz, I. D., Jr., & Petsko, G. A. (1984) *Biochemistry 23*, 2849–2857.

Varadarajan, R., Szabo, A., & Boxer, S. G. (1985) *Proc. Natl. Acad. Sci. U.S.A. 82*, 5681–5684.

Varadarajan, R., Lambright, D. G., & Boxer, S. G. (1989) *Biochemistry 28*, 3771–3781.

Young, R. D., & Bowne, S. F. (1984) *J. Chem. Phys. 81*, 3730–3737.

Young, R. D., Frauenfelder, H., Johnson, J. B., Lamb, D. C., Nienhaus, G. U., Philipp, R., & Scholl, R. (1991) *Chem. Phys. 158*, 315–327.